Biased localization of actin binding proteins by actin filament conformation

Andrew R Harris[1], Pamela Jreij[1], Brian Belardi[1], Andreas Bausch[3], Daniel A Fletcher[1,2,4]*

[1]Department of Bioengineering and Biophysics Program, University of California, Berkeley, 648 Stanley Hall MC 1762, Berkeley, CA 94720, USA

[2]Biological Systems and Engineering Division, Lawrence Berkeley National Laboratory, 648 Stanley Hall MC 1762, Berkeley, CA 94720, USA

[3]Lehrstuhl für Biophysik (E27), Technische Universität München, Garching 85748, Germany.

[4]Chan Zuckerberg Biohub, San Francisco, CA 94158

*Daniel A Fletcher, fletch@berkeley.edu

ABSTRACT

The assembly of actin filaments into distinct cytoskeletal structures plays a critical role in cell movement, shape change, and mechanics, but how different sets of proteins localize to these structures within a shared cytoplasm remains unclear. Here, we show that the actin-binding domains of accessory proteins can be sensitive to filament conformational changes induced by perturbations that include other binding proteins, stabilizing drugs, and physical constraints on the filament. Using a combination of live cell imaging and *in vitro* single molecule binding measurements, we demonstrate that the affinity of tandem calponin homology domain (CH1-CH2) mutants varies as actin filament twist is altered, and we show differential localization of native and mutant CH1-CH2 domains to actin networks at the front and rear of motile cells. These findings suggest that conformational heterogeneity of actin filaments in cells could influence the biochemical composition of cytoskeletal structures through a biophysical feedback loop.

INTRODUCTION

Multiple actin cytoskeletal structures co-exist within the cytoplasm, yet they are spatially organized, architecturally distinct, and perform specific functions(Harris et al., 2018; Michelot and Drubin, 2011). In addition to branched actin networks in the lamellipodium, and stress fibers in the cell body, advances in both optical and electron microscopy continue to reveal more details about the organization and assembly a broader range of actin structures, including filopodia(Svitkina et al., 2003), asters and stars(Fritzsche et al., 2017), podosomes(Luxenburg et al., 2007) and patches(Young et al., 2004). In each of these structures, the interaction of actin filaments with a vast set of ancillary proteins promote the formation of distinct cytoskeletal architectures.

Interestingly, common probes for f-actin, including GFP-tagged actin, small actin-binding peptides (lifeact(Riedl et al., 2008), f-tractin(Schell et al., 2001), affimers(Lopata et al., 2018)) and phallotoxins(Yamashiro et al., 2019), do not distribute evenly on different actin cytoskeletal structures(Belin et al., 2014; Melak et al., 2017; Munsie et al., 2009). Similar observations have been made for fluorescent fusions to minimal actin binding domains from different proteins(Tsujioka et al., 2012; Washington and Knecht, 2008). Mechanistically, these results have been ascribed to the complex and competitive interactions between side binding proteins(Christensen et al., 2017; Gateva et al., 2017), the effect of actin nucleators(Mizuno et al., 2018; Risca et al., 2012), and the kinetic properties of the reporting probe(Maiuri et al., 2015; Yamashiro et al., 2019). However, other properties of actin filaments, including its conformational state, could differ among cytoskeletal structures and be detected by actin-binding proteins to bias their localization.

Several studies have indicated that the conformational state of an actin filament is polymorphic(Egelman et al., 1982; Galkin et al., 2010b; Kozuka et al., 2006) and that actin filaments exist in a range of different ‘flavors’, including different their nucleotide state(Pfaendtner et al., 2009), oxidative state(Hung et al., 2011) and twisted states(Galkin et al., 2010b; Jégou and Romet-Lemonne, 2016; Jegou and Romet-Lemonne, 2019). Actin binding proteins have also been shown to modulate filament structural conformations either as part of their regulatory activity or as a means for allosteric cooperative binding to actin(Ngo et al., 2016; Sharma et al., 2010; Umeki et al., 2016). In addition to effects of protein binding, mechanical perturbations to actin filaments such as torques, tension and bending have been suggested to influence protein interactions with filaments, including the binding of the Arp2/3 complex(Risca et al., 2012) and severing activity of the protein cofilin(Hayakawa et al., 2011; Mizuno et al., 2018; Wioland et al., 2019). Together, these observations suggest that different conformations of f-actin, induced either mechanically or biochemically, could impact the affinity of actin binding proteins for f-actin.

We sought to investigate whether filament conformational changes could be sensed by a common class of actin binding domain, tandem calponin homology domains (CH1-CH2), and whether affinity changes for different conformations could be responsible for biasing the localization of CH1-CH2-containing proteins to different actin structures in cells. Using a combination of live cell imaging and *in vitro* single molecule binding affinity measurements, we find that mutants of the actin-binding

domain of utrophin (CH1-CH2) localize to different actin structures and exhibit differing binding affinities for actin filaments whose conformational state has been altered biophysically and biochemically. We also show that this mechanism extends to native actin-binding domains, suggesting that sensitivity to actin filament conformational states could be playing an important role in the organization and regulation of actin binding proteins in actin filament structures.

RESULTS

Mutants of the actin binding domain of utrophin localize to different actin structures

CH1-CH2 domains are found in many actin crosslinking and regulatory proteins(Harris et al., 2019) including α-actinins in stress fibers(Tojkander et al., 2012) and filamins in the actin cortex(Biro et al., 2013). The actin binding domain of utrophin (CH1-CH2) is used as a generic marker for f-actin(Burkel et al., 2007), which raised the question of whether it uniformly labels all filaments in cells or might be sensitive to filament conformational heterogeneity. Recent cryo-Electron Microscopy studies have mapped the interacting residues between the actin binding domain from filamin A and f-actin(Iwamoto et al., 2018), and between the actin binding domain of utrophin and f-actin to 3.6Å resolution(Kumari et al., 2019). We chose to examine residues predicted to lie within actin binding surface 2 (ABS2) on utrophin CH1(Iwamoto et al., 2018), at the CH1-CH2 domain interface(Galkin et al., 2010a; Harris et al., 2019) and within the n-terminal flanking region(Avery et al., 2017; Harris et al., 2019; Singh et al., 2017), which we had found altered actin-binding affinity in a previous study (Harris et al., 2019).

We first compared the localization of binding interface mutations to that of the actin binding domain of utrophin (utrnWT) in both HeLa cells and PLB neutrophils, which have clearly distinct actin structures (Fig 1, Fig S1). Interestingly, we observed several combinations of mutations that caused significant changes in localization relative to utrnWT (see *Materials and Methods, Engineering utrn ABD affinity and specificity*). The mutations Q33A T36A K121A caused an increased enrichment to lamellipodial actin (Fig 1A, Movie S1, Movie S2), while Q33A T36A G125A L132A was comparatively enriched at the rear of the cell (Fig 1B). We have previously shown that truncating the n-terminal region prior to CH1, Δ-nterm Q33A T36A, changes binding to focal adhesions in HeLa cells(Harris et al., 2019) (Movie S3). This mutant was more evenly distributed at the rear and front of migrating neutrophils compared to utrnWT (Fig 1C, Movie S4). We measured the binding affinity of each of these mutants using *in-vitro* co-sedimentation and found them all to be similar (K_d / K_d *utrnWT*) – within ~2 fold of each other (Fig 1D, Fig S2). Furthermore, the differences in localization between these particular mutants was not directly correlated with bulk binding affinity (Fig 1D), suggesting additional mechanisms influence their localization. Subsequently, we refer to the minimal actin binding domain of utrophin as utrnWT, Q33A T36A K121A mutant as utrnLAM, the Δ-nterm Q33A T36A mutant as utrnΔN and the Q33A T36A G125A L132A mutant as utrnSF.

Single molecule dwell times report complex behavior of utrophin mutants

We entertained the notion that differences in localization of these domains arises due to a bias in binding affinity for actin filaments in each specific network – which we refer to as specificity. We sought to characterise the binding properties of each mutant in more detail *in vitro*. Previously, single molecule kinetic measurements have been used to investigate the binding properties of actin severing proteins(Jansen et al., 2015), formins(Bombardier et al., 2015), cofilin(Hayakawa et al., 2014) and the actin binding domain of α- catenin(Hansen et al., 2013). For α-catenin, the binding dwell time

(inverse of the off-rate) of single molecules followed a two-timescale binding behaviour, in which the binding dwell times increase as a function of concentration of the domain added. This cooperative change in dwell time was reported to be due to structural changes in f-actin that are induced by α-catenin's actin binding domain binding to f-actin(Hansen et al., 2013). Dynamic chances in actin filament conformation in response to biochemical perturbations have also been measured using single molecule FRET measurements on dual-labelled actin monomers(Kozuka et al., 2006). Therefore, to obtain a detailed understanding of the actin-binding kinetics of our different mutants and potential effects of actin structural conformation on binding, we used a TIRF-based single molecule binding assay to measure binding dwell times (Fig 2A, *Materials and Methods, In vitro single molecule binding kinetics assay*).

We compared the distribution and lengths of binding dwell times for the different mutants identified in our first screen. The average dwell times were similar between utrnWT ($\tau_{av\ utrnWT}$ = 1.1sec), utrnLAM ($\tau_{av\ utrnLAM}$ = 1.3sec) and utrnΔN ($\tau_{av\ utrn\Delta N}$ = 0.8sec) (Fig 2B). In contrast, utrnSF had a longer mean dwell time ($\tau_{av\ utrnSF}$ = 4.6sec), indicating that this mutant turned over more slowly. For all of the mutants tested, the distribution of binding dwell-times was well characterised by a double exponential fit and hence a two-timescale binding model (Fig 2C, 2D, Fig S3A-C, *materials and methods - In vitro single molecule binding kinetics assay*). By comparison, the actin binding probe lifeact was well characterised by a single exponential (Fig S3 D-F), confirming that the mechanisms of binding for CH1-CH2 domains is more complex than that of the short peptide. The binding dwell-time of single molecules for utrnWT did not increase as a function of the concentration of dark protein added to the assay (Fig S3C), suggesting that utrnWT did not induce significant structural changes into the actin filament upon binding, unlike the α-catenin actin binding domain[49].

The cumulative distribution function (CDF) of binding dwell-times of the different mutants displayed more detailed differences (Fig 2 C-H). utrnWT (Fig 2C) and utrnΔN (Fig 2D) had two timescales that were more distinct than that of utrnLAM, which was comparatively flatter (Fig 2 C,D,H, characterised by a smaller difference in the two timescales $\tau_2/\tau_{1\ utrnWT}$ = 7.8, $\tau_2/\tau_{1\ utrnLAM}$ = 4.8, $\tau_2/\tau_{1\ utrn\Delta N}$ = 6.0, and a reduction in the τ_1 amplitude, $a_{1\ utrnWT}$ = 0.8, $a_{1\ utrnLAM}$ = 0.7, $a_{1\ utrn\Delta N}$ = 0.8). Removing the Q33A T36A mutations from utrnSF and utrnLAM reduced the overall dwell-time of both (Fig 2E), suggesting that residues within ABS2 and the n-terminal flanking region were indeed important for direct interactions with actin and their localisation.

Filament stabilization by Jasplakinolide but not phalloidin alters utrophin ABD mutant dwell time

We next tested whether stabilization of actin filaments with the small molecules phalloidin and jasplakinolide, which have different effects on actin filament structural conformation(Kumari et al., 2019), altered the binding dwell-times of the different utrophin mutants (Fig 3A). We first introduced 1μM phalloidin into our single molecule binding assay after filaments were attached to the surface of the coverslip, and we found that it had no effect on the binding dwell-time of either utrnWT (Fig 3B, p=0.14), utrnLAM (Fig 3C, p=0.50), or utrnΔN (Fig 3D, p=0.83). In contrast, introduction of 1μM

of the actin stabilizing agent jasplakinolide affected both utrnWT and utrnLAM, making the dwell-time of single molecules shorter in both cases ($\tau_{1\ utrnWT}$ = 0.42 sec, $\tau_{1\ utrnWT+jasp}$ = 0.27 sec, p=0.05, $\tau_{1\ utrnLAM}$ = 0.63 sec, $\tau_{1\ utrnLAM+jasp}$ = 0.29 sec, p<0.05, Fig 3E,F,G). Interestingly, the effect of jasplakinolide was stronger on utrnLAM (~53% reduction in dwell time) than it was on utrnWT (~36% reduction in dwell time), suggesting that each mutant had a different specificity for jasplakinolide stabilized f-actin. Surprisingly, jasplakinolide treatment had little effect on the binding dwell time of utrnΔN (p=0.09, Fig 3D-G). This result suggests that this mutant was insensitive to actin filament conformational change induced by jasplakinolide.

Filament binding by both cofilin and drebrin alters utrophin ABD mutant dwell times

In addition to the small molecules phalloidin and jasplankinolide, several actin binding proteins have been shown to impact filament structure. Cofilin is an actin severing protein that breaks actin filaments by forming discontinuities in filament mechanical properties(De La Cruz, 2009; Wioland et al., 2019). Non-continuous mechanical properties are caused by local changes in filament twist induced by cofilin binding, which change the helical half pitch of f-actin from a mean of ~36nm to ~27nm(Sharma et al., 2010). Given our observations that utrophin ABD mutants were sensitive to actin filament conformation induced by jasplakinolide, we investigated how the different utrophin ABD mutants interacted with cofilin.

First, we measured the severing activity of cofilin in the presence of different utrophin mutants (Fig 4A). We found that introducing 200nM of each of the different mutants reduced the severing rate of 75nM cofilin(Hansen et al., 2013), likely due to direct competition for a similar binding site on f-actin (Fig 4B). Next, we sought to test whether conformational changes induced by cofilin binding impacted the dwell time of the different mutants. We used a dual-color single molecule binding assay with a low concentration of labelled cofilin (10nM), which is not sufficient to drive filament severing, and single molecule levels of utrophin mutant ABD. We then sorted the utrophin mutant ABD single molecule binding events based on their distance from cofilin molecules(Hayakawa et al., 2014), which we were able to localize with a precision of ±30nm (Fig 4C). Since structural changes in actin induced by cofilin are reported to propagate locally, distances ranging from 1-2 subunits(Huehn et al., 2018, 2020), we considered single molecule binding events within 30nm from a cofilin binding event to be 'near' and those beyond 30nm to be 'far'. Average dwell times (τ_{av}) of utrn ABD mutants 'far' from cofilin were similar to our initial measurements in the absence of cofilin ($\tau_{av\ utrnWT\ far}$ = 1.1sec, $\tau_{av\ utrnLAM}$ = 1.3sec, $\tau_{av\ utrnΔN}$ = 1.1sec), while dwell times of both utrnWT (Fig 4D) and utrnLAM (Fig 4E) 'near' cofilin were significantly longer lived (35% and 33% increase in τ_{av} respectively), even though they constituted a small fraction of total recorded events (~1% of total events). In contrast, average dwell times for utrnΔN 'near' cofilin were more similar to those 'far' from cofilin (9% decrease in τ_{av}) (Fig 4G), suggesting that utrnΔN binding was less sensitive to structural changes induced by cofilin binding.

While cofilin shortens the helical half pitch on actin, the actin binding protein drebrin extends the helical half pitch of an actin filament to a mean of ~40nm(Grintsevich et

al., 2010; Sharma et al., 2012, 2010). Since drebrin does not sever filaments, we were able to use higher concentrations of drebrin and include all binding dwell times in our analysis. We tested the effect of 200nM drebrin1-300 and found that drebrin binding reduced the dwell time of both utrnWT and utrnLAM ($\tau_{1\ utrnWT}$ = 0.42 sec, $\tau_{1\ utrnWT+dreb}$ = 0.34 sec, $p<0.05$, $\tau_{1\ utrnLAM}$ = 0.63 sec, $\tau_{1\ utrnLAM+dreb}$ = 0.45 sec, $p<0.05$) (Fig 4H). In addition, drebrin binding also had a smaller but significant effect on the binding lifetime of utrnΔN ($\tau_{1\ utrnΔN}$ = 0.39 sec, $\tau_{1\ utrnΔN+dreb}$ = 0.32 sec, $p<0.05$ Fig 4I-K).

Taken together these results show that structural changes induced by actin binding proteins have an allosteric effect on the kinetic properties of the mutant actin binding domains that we tested, while the domains alone did not bind cooperatively through an allosteric mechanism. This effect depended on the context of conformational change, in this instance under-twisting versus over-twisting of f-actin.

Myosin activity changes the localization and dwell time of utrophin ABD mutants

While cofilin locally remodels actin filaments near the leading edge of migrating cells, myosin localizes to the rear of migrating cells and generates contractile forces needed for cell migration(Bergert et al., 2015; Wilson et al., 2013). Motivated by the differential front-back localization of the utrophin ABD mutants (observed in Fig 1), we tested if myosin activity influenced the binding of purified forms of the utrophin mutants *in-vitro* (Fig 5). First, we generated contractile actin networks in vitro using myosin II filaments and α-actinin (Fig 5A). In comparison to a control network (Fig 5B), we found that there were only subtle differences in the localization of utrnWT and utrnLAM (Fig 5C). In contrast, utrnΔN was more enriched in actomyosin clusters that utrnWT (Fig 5D). utrnWT and utrnSF displayed the most dramatic differences in localization in actin networks (Fig 5E).

Interestingly, no significant differences in localization could be observed in gels where contractility was inhibited by blebbistatin (Fig 5F, 5G), suggesting that active myosin was required to cause changes in localization. To investigate the role of myosin activity further, we measured the single molecule dwell times of utrophin ABD mutants in the presence of the myosin fragment Heavy Meromyosin (HMM). We found that utrnWT (Fig 5H) and utrnLAM (Fig 5I) displayed a reduced dwell time in the presence of HMM ($\tau_{1\ utrnWT}$ = 0.42 sec, $\tau_{1\ utrnWT+HMM}$ = 0.24 sec, $p<0.05$, $\tau_{1\ utrnLAM}$ = 0.63 sec, $\tau_{1\ utrnLAM+HMM}$ = 0.28 sec, $p<0.05$). However, HMM binding had no effect on the binding lifetime of utrnΔN ($p=0.25$ Fig 4J-M).

Physical confinement of actin alters dwell time of utrophin ABD mutants

Given that conformational changes in f-actin induced by both small molecules and binding proteins impacted the dwell times of utrophin mutants, we next sought to investigate how general this mechanism might be. We tested whether physical constraints on actin filaments to the glass surface influenced the dwell time of single molecules in our assay. To investigate this, we built on our combined single molecule dwell time measurements (kinetics) with sub-pixel localisation measurements (STORM) used in our cofilin analysis, to generate images of localized binding dwell-times on actin filaments, an approach we refer to as kSTORM (Fig 6A).

Using kSTORM, we were able to create filament images with a pixel size of 40nm (close to the canonical helical half pitch of f-actin ~36nm (Fig 6B)) and color coded the images based on dwell time of the three different utrophin ABD mutants. We observed that the dwell time of utrnΔN was uniformly distributed across filaments (Fig 6C). In contrast, dwell times appeared to cluster for utrnWT (Fig 6D) and utrnLAM (Fig 6E), with short dwell times (<1sec, blue arrowheads) and long dwell times (>1sec, yellow arrowheads) separating into distinct regions. We hypothesize that as actin filaments are bound to the surface of the flow chamber they adopt a bias for different structural conformations, similar to the dynamic conformational changes in f-actin structure that have been observed using single molecule FRET measurements(Kozuka et al., 2006). This in turn causes clustering of actin binding domain dwell times. These results suggest that mechanical constraint on actin filaments can locally impact the dwell times of different actin binding domain mutants and their segregation into distinct regions.

Native CH1-CH2 domains also display biased localization to different actin structures

Having identified that utrophin ABD mutants localize to different subcellular actin structures and that their binding affinity is altered by changes in actin filament conformation, we wondered if native CH1-CH2 domains displayed similar characteristics. We screened the localization of native CH1-CH2 domains relative to the actin binding domain of utrophin (Fig S4). Native CH1-CH2 domains displayed a range of actin binding affinities, which we assessed from the relative pools of protein on actin and in the cytoplasm in live cells(Harris et al., 2019). We also found that several native CH1-CH2 domains displayed enhanced localization to specific actin structures (Fig 7, FigS4). For example, the actin binding domain of dystonin/BPAG1, a protein that links the actin cytoskeleton to other cytoskeletal networks(Young and Kothary, 2007), was enriched on stress fibers in HeLa cells (Fig 7A, Movie S5). In contrast, the ABD of nesprin II, a protein that links the actin cytoskeleton to the interior of the nucleus(Davidson et al., 2019), was enriched in the lamellipodium in both HeLa cells (Fig 7B, Movie S6) and PLB neutrophils (Fig 7C, Movie S7). These results show that native CH1-CH2 domains, in addition to having different overall affinities, show preferential binding to specific actin structures in cells.

DISCUSSION

By using a combination of live cell imaging, *in-vitro* characterisation, and single molecule binding measurements, we showed that utrophin ABD mutants have varying binding affinities for different conformational states of f-actin and localization to actin structures in live cells. We found that two constructs, utrnWT and utrnLAM, had different specificity for structural changes in f-actin, while utrnΔN was largely insensitive to structural changes. These domains responded to biochemical perturbations, regulatory protein binding and interestingly, mechanical constraints on f-actin.

The identification of specificity of actin binding domains to different actin conformations and actin networks has two broad implications for understanding cytoskeletal physiology. Firstly, in addition to generating mutant actin binding domains from utrophin, we tested the localisation of native CH1-CH2 domains. Many of these domains displayed differences in binding affinity, characterised by differences in cytoplasmic signal (Fig S4), but several actin-binding domains, including nesprin II CH1-CH2 and BPAG1 CH1-CH2 displayed differences in localisation to actin structures. These observations highlight that small differences in sequence between native domains are important for both the affinity and specificity to different actin structures and has broader implications for the activity of full-length actin regulatory proteins. One example of this is indeed nesprin II, which has been shown to localise to the front of the nucleus as cells migrate through small constrictions(Davidson et al., 2019). This localisation was dependent on the presence of the actin-binding domain, suggesting that conformational sensing could help to spatially organise this actin binding protein for its specific function. The broader notion that some actin binding proteins modulate actin filament structure (such as cofilin, formins and myosin), while others can be sensitive to it (CH1-CH2 contain proteins), highlights the role of the actin cytoskeleton as a signalling substrate in its own right, which likely has functional significance for a range of biological processes. Secondly, it is interesting to speculate that CH1-CH2 domains could be used to engineer probes for different structural states of f-actin for use both in vitro and in vivo. In fact, although utrnWT has been commonly used as a marker for f-actin(Burkel et al., 2007), it has also been reported to localize more preferentially to the trailing edge of migrating cells(Fritz-Laylin et al., 2017). C-terminal truncated forms of utrnWT have also been used for labelling of nuclear actin filaments(Belin et al., 2014) and direct fusions to GFP via a helical linker have been used in fluorescence polarization studies(Nakai et al., 2019). We have now shown that distinct mechanisms and residues control both affinity (our previous work(Harris et al., 2019)) and specificity (this work), suggesting that it should be possible to engineer probes with a range of desired properties for cell biological studies(Belardi et al., 2019; Harris et al., 2019).

It is important to note that the actin filament conformation-induced differences in ABD localization we report here are distinct from differences in localization that can arise from proteins with different bulk actin-binding affinities. Previous work has shown that high affinity actin-binding proteins such as myosin are depleted from dynamic actin networks due to their slow turnover rate(Maiuri et al., 2015; Yamashiro et al., 2019). Consistent with this finding, some of the mutants generated in our initial screen also

had a high f-actin binding affinity and displayed differences in localisation (K_d / K_d *utrnWT* ~0.03, utrn Q33A T36A(Harris et al., 2019), Fig S5), being depleted from dynamic actin networks. However, by engineering mutant actin binding domains to have affinities similar to that of utrnWT (Fig 1), we are able to specifically identify preferential binding to actin filaments structures independent of bulk affinity differences. Indeed, when we measured the dynamics of our mutant ABDs (utrnWT, utrnLAM and utrnΔN) in live cells using FRAP (Fig S5, *Materials and Methods*) and single molecule photoactivation (Fig S6, *Materials and Methods*), we found their turnover rates in to be very similar. In particular, single molecule kinetics in live cells were indistinguishable between utrnWT and utrnLAM (p=0.12,) when f-actin structures were homogenised with 50μM Y27632 treatment (depolymerises stress fibers, Fig S6). In fact, utrnΔN turned over slightly more slowly than utrnWT despite its comparative enrichment to more dynamic actin structures (Fig S6E, Fig 1C,D). It is therefore likely that specificity of actin binding proteins combines with their overall bulk binding affinity to generate a rich landscape of actin binding properties and localizations. For example, while myosin binds with high affinity, it has also been shown to bind cooperatively to actin filaments(Prochniewicz et al., 2010) and displays context dependent catch bonding behaviour(Schiffhauer et al., 2016; Uyeda et al., 2011). In addition, lifeact is highly dynamic but does not bind to stressed actin decorated with cofilin(Munsie et al., 2009) or jasplakinolide stabilized actin(Kumari et al., 2019).

Consistent with this notion, we showed that modification of filaments by the actin-stabilizing drugs jasplakinolide and phalloidin have different effects on the binding dwell-time of utrophin ABD mutants. Recent evidence has suggested that jasplakinolide preferentially biases one state of f-actin, stabilizing the D-loop from subdomain 2 in a more open configuration(Pospich et al., 2019), which may partially explain our observations. CH1-CH2 domains have been shown to bind actin by making contacts both on and between actin subunits within the same protofilament(Iwamoto et al., 2018; Kumari et al., 2019) (n and n+2). The n-terminal flanking region contacts the n-terminal actin subunit, ABS2 binds within the cleft between the two subunits (where subdomain 2 from subunit n, contacts subdomain 1 from n+2) and ABS2' contacts subunit n+2. Making several contacts on and between neighbouring f-actin subunits could explain why utrophin's ABD is sensitive to filament level structural changes induced by these small molecule agents. Indeed, the K121A mutation in utrophin corresponds to a key interaction with subdomain 2 and may explain why mutating this residue changes the specificity to jasplakinolide-stabilized actin. This particular effect it titratable, with the K121A mutant being more sensitive to jasplakinolide than utrnWT, which displayed a more modest response. Sequence alignment of native CH1-CH2 domains revealed that this residue is well conserved between domains, though some differences do exist (Fig 7D). Interestingly, K121 is changed to serine in nesprin II which also enriched to lamellipodial actin in a similar fashion to utrnLAM (Q33A T36A K121A). In our previous work we have shown that the n-terminal flanking region is important for localisation of CH1-CH2 domains. In particular, Filamin B which has a short n-terminal flanking region displayed a similar localisation pattern at focal adhesions to utrnΔN(Harris et al., 2019) (Fig 7D). Here, we extend this observation by showing that this region also appears to have a crucial

role in actin filament conformational sensing. In all of the conditions tested utrnΔN showed little to no difference in binding dwell time, suggesting it is largely insensitive to differences in f-actin conformation.

In addition to actin drugs, we show that actin binding proteins that modify actin filament conformations such as drebrin, myosin, and cofilin, impact the binding affinity of the different utrophin mutants. However, protein-induced conformational changes are not required to alter the binding kinetics of our utrn ABD mutants. Indeed, we make the surprising observation using kSTORM that dwell times on actin filaments physically confined to a glass surface show spatial nonuniformity and clustering for utrnWT, utrnLAM but not for utrnΔN. What is the mechanism of this clustering and how does it relate to filament conformational state? Actin binding proteins that change the helical pitch of actin exert a force on the filament, and for cofilin, drebrin and formins, this is a torque(Mizuno et al., 2018; Wioland et al., 2019). Myosin II steps at a distance shorter than the helical half pitch of an actin filament and filaments gliding on a myosin coated surface also spiral(Sase et al., 1997; Suzuki et al., 1996). Since actin filaments are inherently helical in nature, torsion and bending are believed to be coupled to twisting(Enrique et al., 2010; Risca et al., 2012). It is therefore possible that filament structural conformations are biased by physical forces as they are tethered to the bottom of the flow chamber in a particular configuration, which could result in the two timescales of binding observed for the utrophin mutants and spatial clustering. Consistent with this, actin filament conformation was shown to be dynamic using FRET measurements of doubly-labelled actin monomers within filaments, in a similar assay(Kozuka et al., 2006). The D-loop from subdomain 2 in f-actin is also suggested to be flexible. One possibility is that this region be biased by actin filament confinement, bending and twisting resulting in different filament conformational states, resulting in clustering in our assay(Galkin et al., 2012; Orlova and Egelman, 1993). While the mutagenesis study performed here highlights significant new functional roles for different residues on CH1-CH2 domains, further structural work will be needed to identify the binding mechanisms in more detail and how these different regions combine with overall bulk affinity to give rise to unique actin binding properties.

ACKNOWLEGEMENTS

The authors would like to thank Dyche Mullins and members of the Fletcher lab for helpful discussions. This work was supported by grants from NIH (D.A.F). A.R.H. was in receipt of an EMBO long-term fellowship 1075–2013 and HFSP fellowship LT000712/2014. B.B. was supported by the Ruth L. Kirschstein NRSA fellowship from the NIH (1F32GM115091). P.J was supported by an NSF Fellowship and the Berkeley Fellowship for Graduate Studies. A.B. was supported by the Miller Institute for Basic Research at UC Berkeley as a Miller Visiting Professor. We would like to thank Holly Aaron and Feather Ives at the Molecular Imaging Center core facility at UC Berkeley (FRAP experiments were performed at the Molecular Imaging Center using equipment supported by the Helen Wills Neuroscience Institute). We would also like to acknowledge the help of the Marqusee Lab with the CD and melting temperature experiments. D.A.F. is a Chan Zuckerberg Biohub Investigator.

MATERIALS AND METHODS

Cell Culture: HeLa and HEK293 cells were cultured at 37°C in an atmosphere of 5% CO_2 in air in DMEM (Gibco, #10566024) supplemented with 10% FBS (Gibco, #16140071) and 1% Penicillin-Streptomycin (Gibco, #15140122). Adherent cells were passaged at a 1:5 dilution using 0.05% trypsin EDTA (Gibco #25200056). PLB cells were a kind gift from Dr. Sean Collins (UC Davis). PLB cells were cultured in RPMI (Gibco, #11875093) containing 10% FBS and 1% Penicillin-Streptomycin and differentiated into neutrophil like cells by adding 1.5% DMSO for 5-6 days.

Generation of constructs: To visualize the relative localization of fluorescent fusions to actin binding domains, we generated both bi-cistronic expression plasmids for transient transfection and two separate lentiviral plasmids for creating double expression stable cell lines, as described previously (Harris et al., 2019). Mutations to the actin binding domain of utrophin were introduced by PCR. Briefly, two sets of primers containing the point mutation were used to amplify two separate segments of mCherry-utrn ABD (or in some cases EGFP-utrn ABD or RubyII-utrn ABD) which were then re-assembled using Gibson assembly. Transient transfections were performed using effectene (Qiagen, #301425), following the manufacturer's protocol and imaged 24 hours after transfection. For generating stable cell lines GFP-utrn ABD and the construct of interest fused to mCherry were cloned into Lentiviral plasmid pHR. Lentiviruses were then generated by transfecting the plasmids into HEK293 cells for viral packaging. Lentiviral supernatants were collected 48hrs after infection, filtered using a 0.4um filter and used directly to infect the target cell line in a 1:1 ratio with normal culture media. PLB cells were infected by centrifuging cells at 300 rcf for 10 minutes in lentiviral supernatant containing polybrene.

Engineering utrn ABD affinity and specificity: In our previous work(Harris et al., 2019), we have shown that two mechanisms control the overall binding affinity of CH1-CH2 domains. Firstly, CH1-CH2 inter-domain interaction govern the 'openness' of the two CH domains which relieves a steric clash between CH2 and f-actin. Secondly, CH1-factin interactions govern direct binding to f-actin. Each of these mechanisms can be targeted to titrate the overall actin binding affinity of the domains. The double mutant Q33A T36A perturbs interdomain interactions and makes it easier for the actin binding domain of utrophin to transition to an open bound state on f-actin. These mutations caused an increase in actin binding affinity through changes in both on rate and off rate. By combining inter-CH domain interactions with f-actin binding interactions it is possible to create a range of binding properties tuning affinity to be similar whilst probing different regions on utrn ABD to test specificity to binding to different conformations of f-actin.

Cellular confocal imaging: Cells expressing fluorescent fusion proteins were imaged using the following excitation and emission: GFP was excited at 488 nm and emission was collected at 525 nm, mCherry was excited at 543 nm, and emission was collected at 617 nm. Live imaging experiments were performed in normal cell culture media using an OKO labs microscope stage enclosure at 37°C in an atmosphere of 5% CO_2. Cells were imaged on glass bottomed 8 well chambers that had been coated with

10ug/ml fibronectin in PBS for 30minutes. Cells were imaged with a 60x oil immersion objective N.A. 1.4.

Fluorescence Recovery After Photobleaching (FRAP): To assess the turnover kinetics and mobility of utrnABD mutants Fluorescence Recovery After Photobleaching experiments were performed. FRAP measurements were performed specifically on stress fibers in HeLa cells. The turnover of different mutants was measured by bleaching a 6pixel diameter spot (~1µm) using a scanning laser confocal microscope (Zeiss LSM 880 with Airyscan). Fusion constructs to mCherry were used in FRAP experiments. To analyse FRAP data, time lapse stacks were imported into Fiji and bleached regions analysed as ROI. FRAP data were bleaching corrected as previously described(Phair et al., 2003) and the initial rate of recovery found from the initial slope of the recovery curve using MatLab.

Single molecule binding measurements in live cells: To complement the kinetic measurements in live cells using FRAP on stress fibers, we used photoconversion and single molecule binding measurements. Mutants of interested were generated as fusions to mEOS for single molecule photoactivation with TIRF microscopy. Because cells contain a range of different actin structures that could influence the binding kinetics results, we pre-treated cells with 50µM of the ROCK inhibitor Y27632 for 30mins, to depolymerize stress fibers. Single molecules were then activated with a 30ms pulse of 405nm light in TIRF, and then imaged with 561nm excitation at an interval of 50ms. Single molecules were identified and tracked using the TrackNTrace software package(Stein and Thiart, 2016). A custom written MatLab routine was then used to post-process the image tracks and calculate binding dwell- times.

Protein purification and labelling: Actin was purified from rabbit muscle acetone powder (Pel Freez Biologicals, #41995-1) and stored in monomeric form in G-buffer (2mM Tris-Cl pH 8.0, 0.2 mM ATP, 0.5 mM TCEP, 0.1 mM $CaCl_2$) at 4°C. Utrophin's actin binding domain (CH1-CH2) and its associated mutants were expressed recombinantly in E. coli BL21 (DE3) pLysS (Promega, #L1191) and purified using affinity chromatography followed by gel filtration. Proteins were stored in 20 mM Tris-Cl pH 7.5, 150 mM KCL, 0.5 mM TCEP and 0.1 mM EDTA and in the presence of 20% glycerol. Utrophin ABD sequences included a KCK linker (GGSGKCKSA) on the C terminus for labelling. Proteins were labelled using either Alexa 488 C_5 maleimide, Alexa 555 C_2 maleimide or Alexa 647 C_2 maleimide (ThermoFisher, #A10254, #A20346, #A20347) as previously described(Harris et al., 2019). The minimal actin binding portion of drebrin 1-300 was purified using the same strategy. Acanthamoeba α-actinin and Atto-488 cofilin were a kind gift from Peter Bieling (Max Plank Institute of Molecular Physiology, Dortmund).

Surface functionalization and flow well assembly: Crosslinked network and single filament assays were performed in a flow well configuration consisting of a functionalized coverslip and passivated counter-surface assembled using Tesa double sided tape. Glass slides (VWR, #48300-047) were plasma cleaned then passivated using PLL-PEG (g = 3.5). 22x22mm coverslips (Zeiss, #474030-9020-000) were passivated using PEG-silane chemistry(Bieling et al., 2010). Firstly, glass coverslips were cleaned with 3N NaOH, rinsed in miliQ water, piranha cleaned, rinsed and dried,

and then incubated with GOTPS for 1 hour at 75°C. After silanizaion, the coverslips were rinsed in anhydrous acetone and dried. PEG was coupled to the silanized surface by preparing a PEG saturated acetone solution at 95% hydroxy-amino-PEG (Rapp Polymere, #10 3000-20) and 5% biotinyl-amino-PEG (Rapp Polymere, #13 3000-25-20) which was incubated for a minimum of 4 hours at 50°C. PEG passivated coverslips were then rinsed in miliQ and stored at room temperature and used within 1 month.

Total Internal Reflection Fluorescence Microscopy (TIRF): TIRF microscopy was used for measuring single molecule binding kinetics in cells and *in vitro*. The imaging system consisted of a Nikon TIRF inverted scope (Nikon Eclipse Ti, 488/560/642nm OPSL lasers) with perfect focus, a 100x N.A. 1.4 APO TIRF oil objective, and an EMCCD camera (Andor iXon Ultra).

In vitro single molecule binding kinetics assay: To evaluate the binding properties of different utrophin ABD mutants, single molecule binding kinetics were measured. Actin filaments were polymerized at a final concentration of 5 μM at room temperature. To immobilize actin filaments to the surface of the flow chamber, flow wells were first incubated with 10μg/mL streptavidin (Sigma #S0677) for 1 minute, washed with f-buffer and then incubated with 1μM biotin phalloidin, (ThermoFisher #B7474) for 1 minute. Actin filaments were then diluted 50x in fbuffer and immediately introduced into the flow well and allowed to attach for 5 minutes. Remaining filaments were washed away with assay buffer (25mM Immidizole, 25mM KCl, 4mM $MgCl_2$, 1mM EGTA, 1mM DTT and 10μg/mL Beta Casein (Sigma C6905)). Binding proteins were diluted to a sufficiently low concentration to enable the visualisation of single molecules in TIRF, 0.05-10nM in assay buffer. For single molecule kinetic measurements 600 frames were acquired at an interval of ~30-130ms depending on the construct. Single molecules were identified and tracked using the TrackNTrace software package(Stein and Thiart, 2016). A custom written MatLab routine was then used to post-process the image tracks and calculate binding dwell-times. To remove outliers, maximum intensity projections of the image stack were used to identify the filament backbone. An image mask was then generated which filtered out single binding events in the maximum intensity projection which did not reside within filament backbone. Binding measurements were then calculated from the filament masked regions. The population of single molecule binding events for different actin binding mutants were analysed in two different ways. Firstly, the average dwell time (τ_{av}) for the entire population was measured as a metric for bulk binding dwell time. Secondly, the cumulative distribution function of binding dwell times was calculated and fitted with a two-timescale binding model. $(1 - CDF) = a_1 e^{-t/\tau_1} + (1 - a_1) e^{-t/\tau_2}$.

Actin network assays: To generate actin networks, all reagents and binding proteins, excluding g-acitn, were added in presence of AB buffer (25mM Immidizole, 25mM KCl, 4mM $MgCl_2$, 1mM EGTA, 1mM DTT). Actin was then added to initialize network formation. Actin and binding proteins were used at final concentrations of: 12μM actin, 200nM of each fluorescently labelled actin binding domain, 2.5μM α-actinin and 500nM myosin II. Before actin polymerisation, samples were incubated for 5 minutes to allow for the assembly of myosin filaments and homogenized by pipetting to obtain a near uniform myosin filament size before adding to the imaging chamber. Samples were incubated in the imaging chamber for 3 minutes to generate contractile networks

and then images immediately with spinning disc confocal microscopy. To generate non-contractile networks, 50μM blebbistatin was added to the initial mix, which inhibits contractility but not myosin filament assembly.

Actin Filament Binding Assay: Filamentous actin was prepared by polymerizing β-actin at 162 μM for 1.5 hr at room temperature. Various concentrations of f-actin were then combined with 100nM of fluorophore-labeled actin-binding domain in f-buffer. Sub stoichiometric concentrations of actin-binding domains were used in all experiments, such that the assumption of $[\text{f-actin}]_{total} \approx [\text{f-actin}]_{free}$ was valid. After incubation at room temperature for 30 min, f-actin and bound actin-binding domain were pelleted at 150,000 x *g* for 60 min at 4 °C. The supernatants were then collected, and unbound actin-binding domain fluorescence intensity was analyzed using a fluorimeter (Biotek Instruments, Inc.). Normalized bound fractions were fitted with the following equation $I = \frac{a*[f-actin]}{(k_D+[f-actin])}$. Where I is the normalized bound fraction, a is the binding stoichiometry, [f-actin] is the actin concentration and k_D is the dissociation constant.

Statistics: Error bars represent standard error, unless otherwise specified. Statistical significance was determined by a two-tailed student's t-test and assumed significant when $p<0.05$. For single molecule dwell time measurements, individual replicates were considered to be individual imaging chambers (consisting of >1000 binding events) imaged on different days. A minimum of 3 replicates was measured for each condition. For dual single molecule cofilin measurements, coincident events were rare (>1% of total binding events). To compare cofilin data the average dwell time was compared rather than the full fit of the CDF from different replicates.

REFERENCES

Avery AW, Fealey ME, Wang F, Orlova A, Thompson AR, Thomas DD, Hays TS, Egelman EH. 2017. Structural basis for high-affinity actin binding revealed by a β-III-spectrin SCA5 missense mutation. *Nat Commun* **8**:1350.

Belardi B, Hamkins-Indik T, Harris AR, Fletcher DA. 2019. A weak link with actin organizes tight junctions to control epithelial permeability. *bioRxiv* 805689.

Belin BJ, Goins LM, Mullins RD. 2014. Comparative analysis of tools for live cell imaging of actin network architecture. *BioArchitecture* **4**:189–202.

Bergert M, Erzberger A, Desai RA, Aspalter IM, Oates AC, Charras G, Salbreux G, Paluch EK. 2015. Force transmission during adhesion-independent migration. *Nat Cell Biol* **17**:524.

Bieling P, Telley IA, Hentrich C, Piehler J, Surrey T. 2010. Fluorescence microscopy assays on chemically functionalized surfaces for quantitative imaging of microtubule, motor, and+ TIP dynamics. *Methods Cell Biol* **95**:555–580.

Biro M, Romeo Y, Kroschwald S, Bovellan M, Boden A, Tcherkezian J, Roux PP, Charras G, Paluch EK. 2013. Cell cortex composition and homeostasis resolved by integrating proteomics and quantitative imaging. *Cytoskeleton* **70**:741–754.

Bombardier JP, Eskin JA, Jaiswal R, Corrêa Jr IR, Xu M-Q, Goode BL, Gelles J. 2015. Single-molecule visualization of a formin-capping protein 'decision complex'at the actin filament barbed end. *Nat Commun* **6**:8707.

Burkel BM, Von Dassow G, Bement WM. 2007. Versatile fluorescent probes for actin filaments based on the actin-binding domain of utrophin. *Cell Motil Cytoskeleton* **64**:822–832.

Christensen JR, Hocky GM, Homa KE, Morganthaler AN, Hitchcock-DeGregori SE, Voth GA, Kovar DR. 2017. Competition between Tropomyosin, Fimbrin, and ADF/Cofilin drives their sorting to distinct actin filament networks. *Elife* **6**:e23152.

Davidson PM, Battistella A, Déjardin T, Betz T, Plastino J, Cadot B, Borghi N, Sykes C. 2019. Actin accumulates nesprin-2 at the front of the nucleus during confined cell migration. *bioRxiv* 713982.

De La Cruz EM. 2009. How cofilin severs an actin filament. *Biophys Rev* **1**:51–59.

Egelman EH, Francis N, DeRosier DJ. 1982. F-actin is a helix with a random variable twist. *Nature* **298**:131.

Enrique M, Roland J, McCullough BR, Blanchoin L, Martiel J-L. 2010. Origin of twist-bend coupling in actin filaments. *Biophys J* **99**:1852–1860.

Fritz-Laylin LK, Riel-Mehan M, Chen B-C, Lord SJ, Goddard TD, Ferrin TE, Nicholson-Dykstra SM, Higgs H, Johnson GT, Betzig E. 2017. Actin-based protrusions of migrating neutrophils are intrinsically lamellar and facilitate direction changes. *Elife* **6**:e26990.

Fritzsche M, Li D, Colin-York H, Chang VT, Moeendarbary E, Felce JH, Sezgin E, Charras G, Betzig E, Eggeling C. 2017. Self-organizing actin patterns shape membrane architecture but not cell mechanics. *Nat Commun* **8**:14347.

Galkin VE, Orlova A, Egelman EH. 2012. Actin filaments as tension sensors. *Curr Biol* **22**:R96–R101.

Galkin VE, Orlova A, Salmazo A, Djinovic-Carugo K, Egelman EH. 2010a. Opening of tandem calponin homology domains regulates their affinity for F-actin. *Nat Struct Mol Biol* **17**:614–616.

Galkin VE, Orlova A, Schröder GF, Egelman EH. 2010b. Structural polymorphism in F-actin. *Nat Struct Mol Biol* **17**:1318–1323.

Gateva G, Kremneva E, Reindl T, Kotila T, Kogan K, Gressin L, Gunning PW, Manstein DJ, Michelot A, Lappalainen P. 2017. Tropomyosin isoforms specify functionally distinct actin filament populations in vitro. *Curr Biol* **27**:705–713.

Grintsevich EE, Galkin VE, Orlova A, Ytterberg AJ, Mikati MM, Kudryashov DS, Loo JA, Egelman EH, Reisler E. 2010. Mapping of drebrin binding site on F-actin. *J Mol Biol* **398**:542–554.

Hansen SD, Kwiatkowski AV, Ouyang C-Y, Liu H, Pokutta S, Watkins SC, Volkmann N, Hanein D, Weis WI, Mullins RD. 2013. αE-catenin actin-binding domain alters actin filament conformation and regulates binding of nucleation and disassembly factors. *Mol Biol Cell* **24**:3710–3720.

Harris AR, Belardi B, Jreij P, Wei K, Shams H, Bausch A, Fletcher DA. 2019. Steric regulation of tandem calponin homology domain actin-binding affinity. *Mol Biol Cell* mbc. E19-06-0317.

Harris AR, Jreij P, Fletcher DA. 2018. Mechanotransduction by the Actin Cytoskeleton: Converting Mechanical Stimuli into Biochemical Signals. *Annu Rev Biophys* **47**:617–631.

Hayakawa K, Sakakibara S, Sokabe M, Tatsumi H. 2014. Single-molecule imaging and kinetic analysis of cooperative cofilin–actin filament interactions. *Proc Natl Acad Sci* **111**:9810–9815.

Hayakawa K, Tatsumi H, Sokabe M. 2011. Actin filaments function as a tension sensor by tension-dependent binding of cofilin to the filament. *J Cell Biol* **195**:721–727.

Huehn A, Cao W, Elam WA, Liu X, Enrique M, Sindelar CV. 2018. The actin filament twist changes abruptly at boundaries between bare and cofilin-decorated segments. *J Biol Chem* **293**:5377–5383.

Huehn AR, Bibeau JP, Schramm AC, Cao W, Enrique M, Sindelar CV. 2020. Structures of cofilin-induced structural changes reveal local and asymmetric perturbations of actin filaments. *Proc Natl Acad Sci*.

Hung R-J, Pak CW, Terman JR. 2011. Direct redox regulation of F-actin assembly and disassembly by Mical. *Science* **334**:1710–1713.

Iwamoto DV, Huehn A, Simon B, Huet-Calderwood C, Baldassarre M, Sindelar CV, Calderwood DA. 2018. Structural basis of the filamin A actin-binding domain interaction with F-actin. *Nat Struct Mol Biol* 1.

Jansen S, Collins A, Chin SM, Ydenberg CA, Gelles J, Goode BL. 2015. Single-molecule imaging of a three-component ordered actin disassembly mechanism. *Nat Commun* **6**:7202.

Jegou A, Romet-Lemonne G. 2019. The many implications of actin filament helicitySeminars in Cell & Developmental Biology. Elsevier.

Jégou A, Romet-Lemonne G. 2016. Single Filaments to Reveal the Multiple Flavors of Actin. *Biophys J* **110**:2138–2146.

Keep NH, Norwood FL, Moores CA, Winder SJ, Kendrick-Jones J. 1999. The 2.0 Å structure of the second calponin homology domain from the actin-binding region of the dystrophin homologue utrophin. *J Mol Biol* **285**:1257–1264.
Kozuka J, Yokota H, Arai Y, Ishii Y, Yanagida T. 2006. Dynamic polymorphism of single actin molecules in the actin filament. *Nat Chem Biol* **2**:83.
Kumari A, Kesarwani S, Javoor MG, Vinothkumar KR, Sirajuddin M. 2019. Structural insights into filament recognition by cellular actin markers. *bioRxiv* 846337.
Lopata A, Hughes R, Tiede C, Heissler SM, Sellers JR, Knight PJ, Tomlinson D, Peckham M. 2018. Affimer proteins for F-actin: novel affinity reagents that label F-actin in live and fixed cells. *Sci Rep* **8**:6572.
Luxenburg C, Geblinger D, Klein E, Anderson K, Hanein D, Geiger B, Addadi L. 2007. The architecture of the adhesive apparatus of cultured osteoclasts: from podosome formation to sealing zone assembly. *PloS One* **2**:e179.
Maiuri P, Rupprecht J-F, Wieser S, Ruprecht V, Bénichou O, Carpi N, Coppey M, De Beco S, Gov N, Heisenberg C-P. 2015. Actin flows mediate a universal coupling between cell speed and cell persistence. *Cell* **161**:374–386.
Melak M, Plessner M, Grosse R. 2017. Actin visualization at a glance. *J Cell Sci* **130**:525–530.
Michelot A, Drubin DG. 2011. Building distinct actin filament networks in a common cytoplasm. *Curr Biol* **21**:R560–R569.
Mizuno H, Tanaka K, Yamashiro S, Narita A, Watanabe N. 2018. Helical rotation of the diaphanous-related formin mDia1 generates actin filaments resistant to cofilin. *Proc Natl Acad Sci* 201803415.
Munsie LN, Caron N, Desmond CR, Truant R. 2009. Lifeact cannot visualize some forms of stress-induced twisted F-actin. *Nat Methods* **6**:317–317.
Nakai N, Sato K, Tani T, Saito K, Sato F, Terada S. 2019. Genetically encoded orientation probes for F-actin for fluorescence polarization microscopy. *Microscopy* **68**:359–368.
Ngo KX, Umeki N, Kijima ST, Kodera N, Ueno H, Furutani-Umezu N, Nakajima J, Noguchi TQ, Nagasaki A, Tokuraku K. 2016. Allosteric regulation by cooperative conformational changes of actin filaments drives mutually exclusive binding with cofilin and myosin. *Sci Rep* **6**:35449.
Orlova A, Egelman EH. 1993. A conformational change in the actin subunit can change the flexibility of the actin filament. Elsevier.
Pfaendtner J, Branduardi D, Parrinello M, Pollard TD, Voth GA. 2009. Nucleotide-dependent conformational states of actin. *Proc Natl Acad Sci* **106**:12723–12728.
Phair RD, Gorski SA, Misteli T. 2003. Measurement of dynamic protein binding to chromatin in vivo, using photobleaching microscopyMethods in Enzymology. Elsevier. pp. 393–414.
Pospich S, Merino F, Raunser S. 2019. Structural effects and functional implications of phalloidin and jasplakinolide binding to actin filaments. *bioRxiv* 794495.
Prochniewicz E, Chin HF, Henn A, Hannemann DE, Olivares AO, Thomas DD, Enrique M. 2010. Myosin isoform determines the conformational dynamics and cooperativity of actin filaments in the strongly bound actomyosin complex. *J Mol Biol* **396**:501–509.

Riedl J, Crevenna AH, Kessenbrock K, Yu JH, Neukirchen D, Bista M, Bradke F, Jenne D, Holak TA, Werb Z. 2008. Lifeact: a versatile marker to visualize F-actin. *Nat Methods* **5**:605–607.

Risca VI, Wang EB, Chaudhuri O, Chia JJ, Geissler PL, Fletcher DA. 2012. Actin filament curvature biases branching direction. *Proc Natl Acad Sci* **109**:2913–2918.

Sase I, Miyata H, Ishiwata S, Kinosita K. 1997. Axial rotation of sliding actin filaments revealed by single-fluorophore imaging. *Proc Natl Acad Sci* **94**:5646–5650.

Schell MJ, Erneux C, Irvine RF. 2001. Inositol 1, 4, 5-trisphosphate 3-kinase A associates with F-actin and dendritic spines via its N terminus. *J Biol Chem* **276**:37537–37546.

Schiffhauer ES, Luo T, Mohan K, Srivastava V, Qian X, Griffis ER, Iglesias PA, Robinson DN. 2016. Mechanoaccumulative Elements of the Mammalian Actin Cytoskeleton. *Curr Biol*.

Sharma S, Grintsevich EE, Hsueh C, Reisler E, Gimzewski JK. 2012. Molecular cooperativity of drebrin1-300 binding and structural remodeling of F-actin. *Biophys J* **103**:275–283.

Sharma S, Grintsevich EE, Phillips ML, Reisler E, Gimzewski JK. 2010. Atomic force microscopy reveals drebrin induced remodeling of F-actin with subnanometer resolution. *Nano Lett* **11**:825–827.

Singh SM, Bandi S, Mallela KM. 2017. The N-Terminal flanking region modulates the actin binding affinity of the utrophin tandem calponin-homology domain. *Biochemistry* **56**:2627–2636.

Stein SC, Thiart J. 2016. TrackNTrace: A simple and extendable open-source framework for developing single-molecule localization and tracking algorithms. *Sci Rep* **6**:37947.

Suzuki N, Miyata H, Ishiwata S, Kinosita Jr K. 1996. Preparation of bead-tailed actin filaments: estimation of the torque produced by the sliding force in an in vitro motility assay. *Biophys J* **70**:401–408.

Svitkina TM, Bulanova EA, Chaga OY, Vignjevic DM, Kojima S, Vasiliev JM, Borisy GG. 2003. Mechanism of filopodia initiation by reorganization of a dendritic network. *J Cell Biol* **160**:409–421.

Tojkander S, Gateva G, Lappalainen P. 2012. Actin stress fibers–assembly, dynamics and biological roles. *J Cell Sci* **125**:1855–1864.

Tsujioka M, Yumura S, Inouye K, Patel H, Ueda M, Yonemura S. 2012. Talin couples the actomyosin cortex to the plasma membrane during rear retraction and cytokinesis. *Proc Natl Acad Sci* **109**:12992–12997.

Umeki N, Hirose K, Uyeda TQ. 2016. Cofilin-induced cooperative conformational changes of actin subunits revealed using cofilin-actin fusion protein. *Sci Rep* **6**.

Uyeda TQ, Iwadate Y, Umeki N, Nagasaki A, Yumura S. 2011. Stretching actin filaments within cells enhances their affinity for the myosin II motor domain. *PloS One* **6**:e26200.

Washington RW, Knecht DA. 2008. Actin binding domains direct actin-binding proteins to different cytoskeletal locations. *BMC Cell Biol* **9**:10.

Wilson K, Lewalle A, Fritzsche M, Thorogate R, Duke T, Charras G. 2013. Mechanisms of leading edge protrusion in interstitial migration. *Nat Commun* **4**.

Wioland H, Jegou A, Romet-Lemonne G. 2019. Torsional stress generated by ADF/cofilin on cross-linked actin filaments boosts their severing. *Proc Natl Acad Sci* 201812053.

Yamashiro S, Taniguchi D, Tanaka S, Kiuchi T, Vavylonis D, Watanabe N. 2019. Convection-induced biased distribution of actin probes in live cells. *Biophys J* **116**:142–150.

Young KG, Kothary R. 2007. Dystonin/Bpag1—a link to what? *Cell Motil Cytoskeleton* **64**:897–905.

Young ME, Cooper JA, Bridgman PC. 2004. Yeast actin patches are networks of branched actin filaments. *J Cell Biol* **166**:629–635.

FIGURES

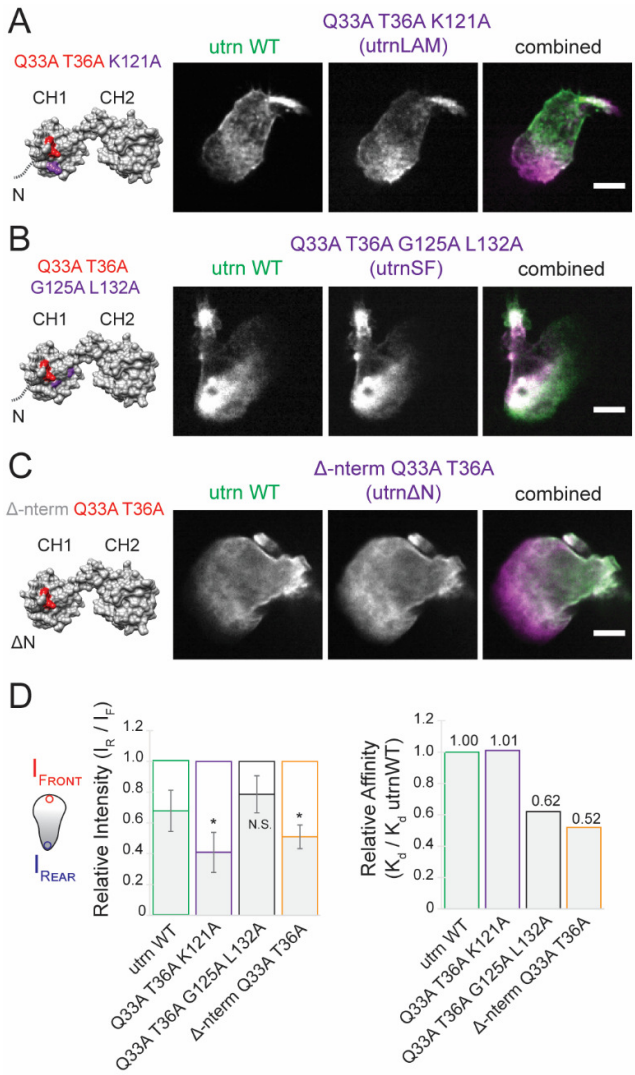

Figure 1: Utrophin CH1-CH2 mutants display differential front-back localization in neutrophils.

Structure of the actin binding domain of utrophin (1QAG (Keep et al., 1999)). The N-terminal flanking region which is not resolved in the crystal structure is indicated by the dashed line. Images show the mutant in magenta compared to utrnWT in green. (A) The mutant utrn Q33A T36A K121A is localized more strongly to the leading edge than utrnWT**.** (B) The mutant utrn Q33A T36A G125A L132A is localized more strongly to the rear of the cell than utrnWT**.** (C) The mutant utrn Δ-nterm Q33A T36A is localized more strongly to the leading edge than utrnWT, similar to utrn Q33A T36A K121A**.** (D) Comparisons of the relative utrn construct intensity at the front and back of migrating neutrophils, calculated by averaging the intensity in 1μm regions at the front and back fo the cell (left). The K_d for each of these constructs normalized to that of utrnWT (right).

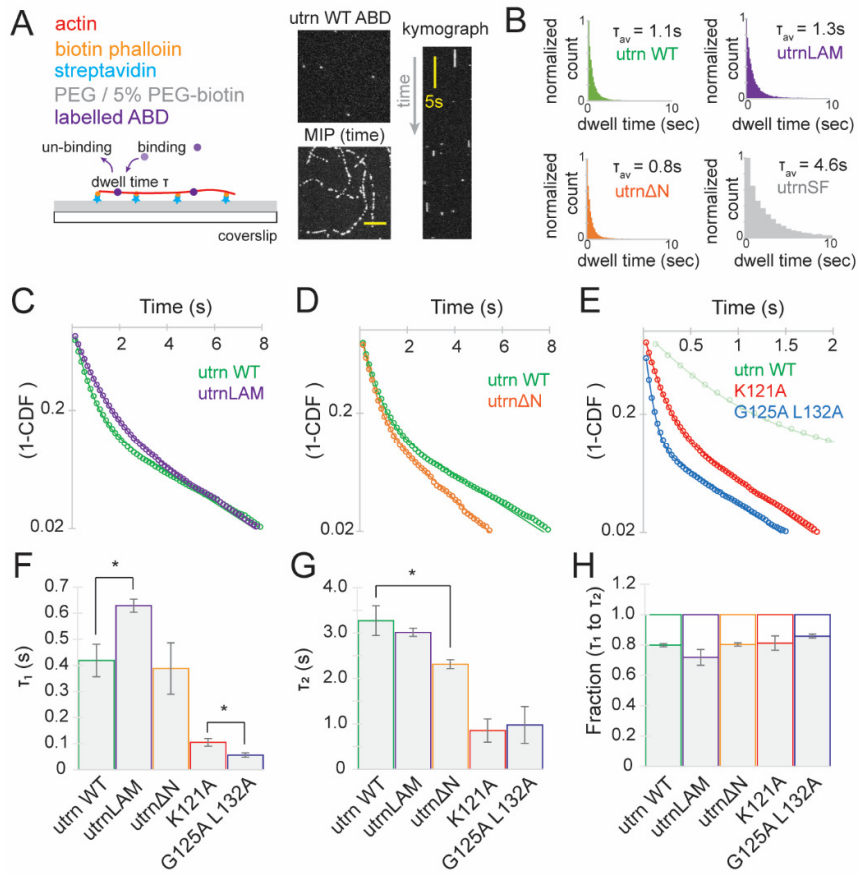

Figure 2: Single molecule kinetic measurements of utrn CH1-CH2 mutants in vitro.

(A) Single molecule binding assay to measure the kinetic properties. Images in the example shown are for utrnWT. Maximum intensity projection through time displays the filament backbones and a kymograph the kinetics of binding. (B) Average binding dwell times for the different CH1-CH2 mutants. (C) Cumulative distribution function for utrnWT and utrnLAM. (D) Cumulative distribution function for utrnWT and utrnΔN. (E) Cumulative distribution function for K121A and G125A L132A. (F) Comparisons of the first timescale τ_1, (G) second timescale τ_2, and (H) relative amplitudes (a_1, $1-a_1$) from a double exponential fit to the cumulative distribution functions for the different constructs.

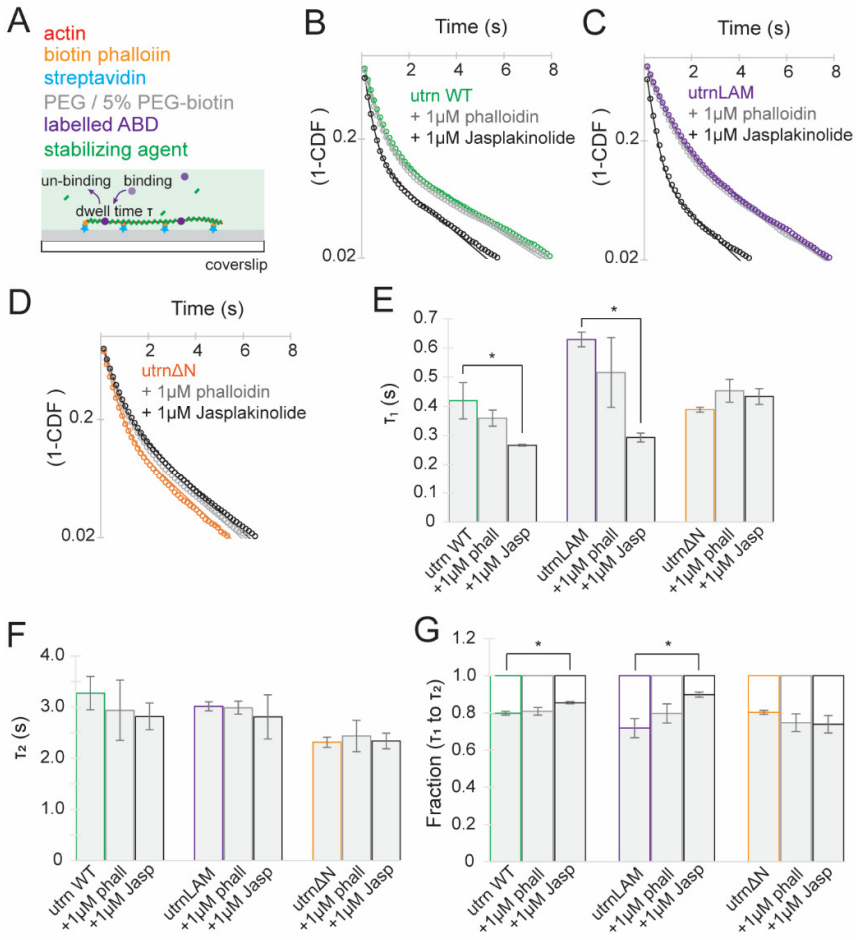

Figure 3: Filament stabilization by Jasplakinolide but not phalloidin alters utrophin ABD mutant dwell time.

(A) Measurement of binding dwell times in the presence of actin stabilizing agents. (B) Cumulative distribution function for utrnWT (green), in the presence of 1μM phalloidin (grey), or 1μM jasplakinolide (black). (C) Cumulative distribution function for utrnLAM (purple), in the presence of 1μM phalloidin (grey), or 1μM jasplakinolide (black). (D) Cumulative distribution function for utrnΔN (orange), in the presence of 1μM phalloidin (grey), or 1μM jasplakinolide (black). (E) Comparisons of the first timescale**,** (F) second timescale**,** and (G) relative amplitudes from a double exponential fit to the cumulative distribution functions for the different constructs and conditions.

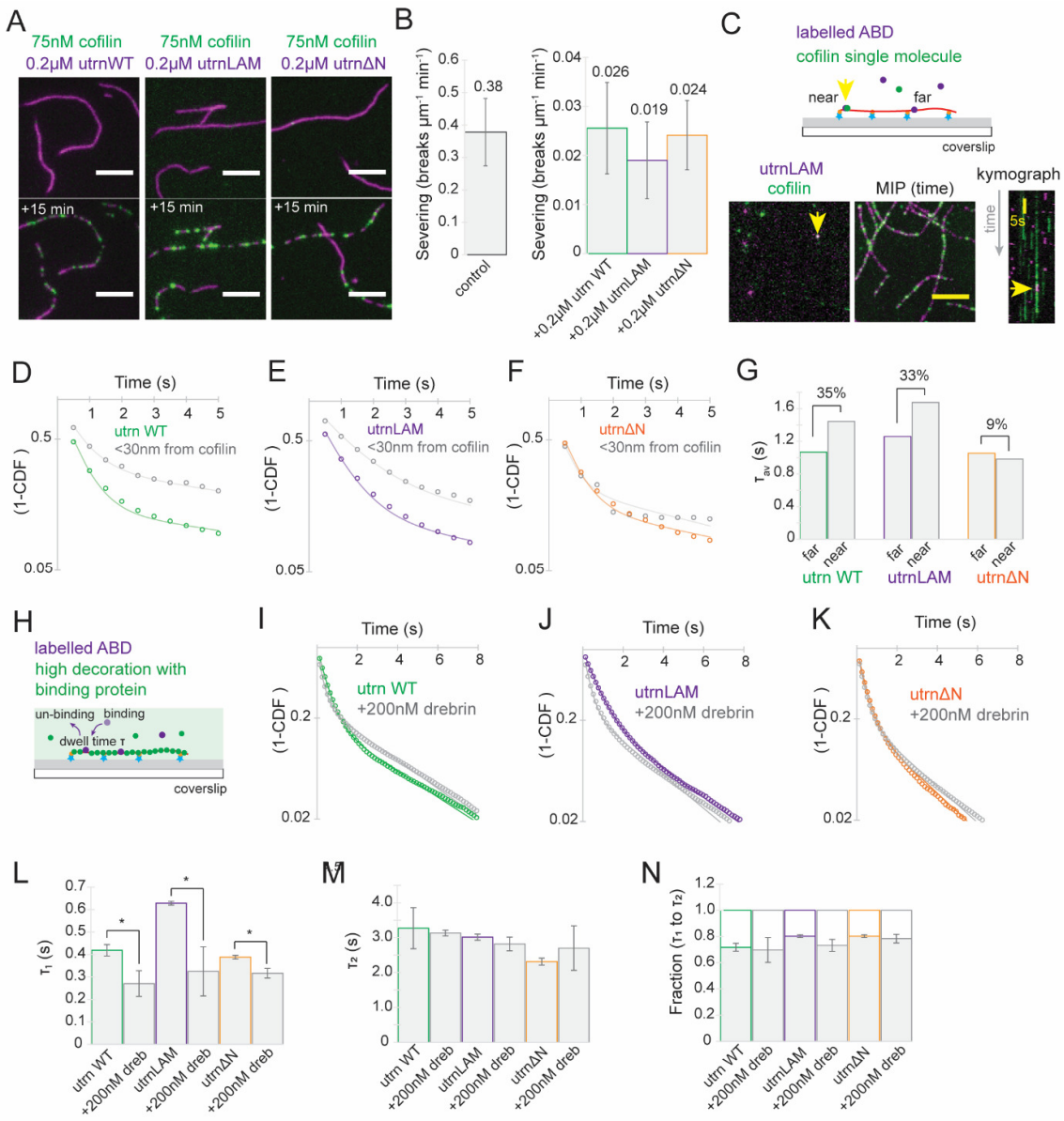

Figure 4: Filament binding by both cofilin and drebrin alters utrophin ABD mutant dwell times.

(A) Actin filament severing by cofilin in the presence of 0.2μM of the different utrophin mutants. (B) Quantification of actin filament severing rate. (C) Dual single molecule colocalization and kinetic measurements at low concentrations of cofilin (10nM) analyzed both near and far from a cofilin binding event. (D) Cumulative distribution functions for molecules near (<30nm) and far (>30nm) from a cofilin binding event for utrn WT, (E) utrnLAM and (F) utrnΔN. (G) differences in average dwell times near and far from a cofilin binding event. (H) Single molecule binding kinetics in the presence of high filament labelling with the actin binding protein drebrin. Cumulative distribution functions for (I) utrnWT, (J) utrnLAM and (K) utrnΔN. (L) Comparisons of the first timescale (M) second timescale and (N) relative amplitudes from a double exponential fit to the cumulative distribution functions for the different constructs.

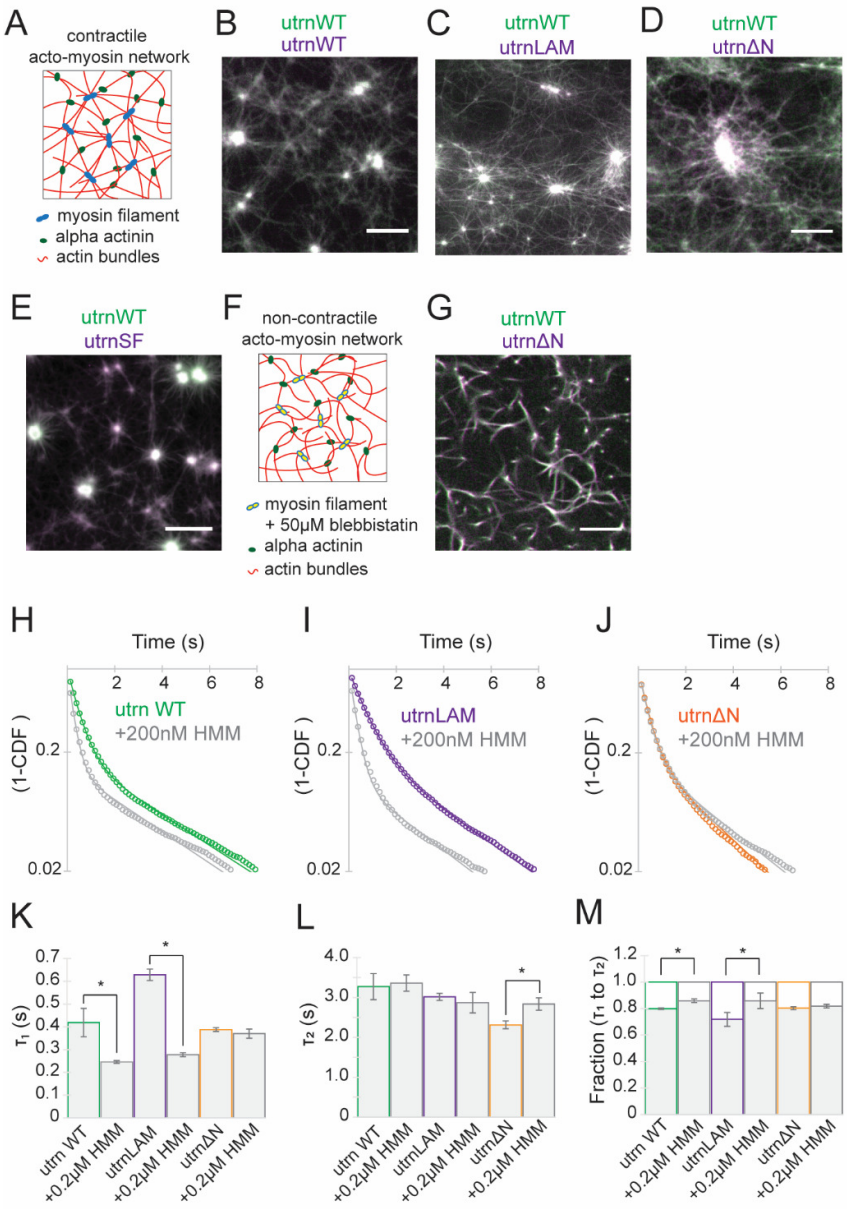

Figure 5: Myosin activity changes localization and dwell time of utrophin ABD mutants.

(A) Generation of contractile acto-myosin networks. Localization of (B) utrnWT, (C) utrnLAM, (D) utrnΔN and (E) utrnSF shown in (magenta) relative to utrnWT (green) in actin networks. (F) Generation of non-contractile actin networks through the addition of 50μM blebbistatin. (G) Localization of utrnΔN (magenta) relative to utrnWT (green) in a non-contractile gel. Cumulative distribution function for (H) utrnWT and (I) utrnLAM and (J) utrnΔN in the presence of 200nM HMM. (K) Comparisons of the first timescale, (L) second timescale, and (M) relative amplitudes from a double exponential fit to the cumulative distribution functions for the different constructs.

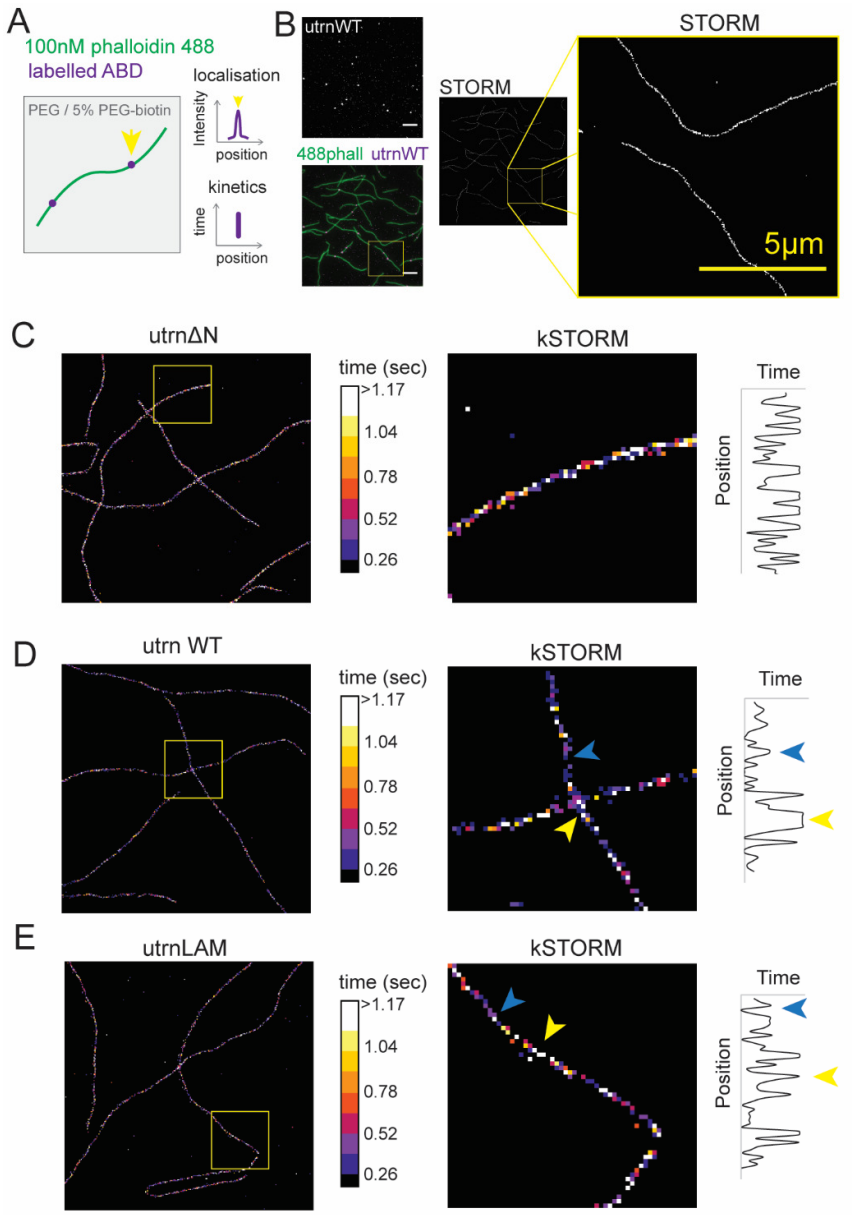

Figure 6: Physical constraints on actin alters dwell time of utrophin ABD mutants.

(A) kSTORM combines subpixel localization measurements with kinetics. (B) Example STORM reconstructions of single molecule measurements from utrnWT. (C) kSTORM images for utrnΔN, (D) utrnWT and (E) utrnLAM.

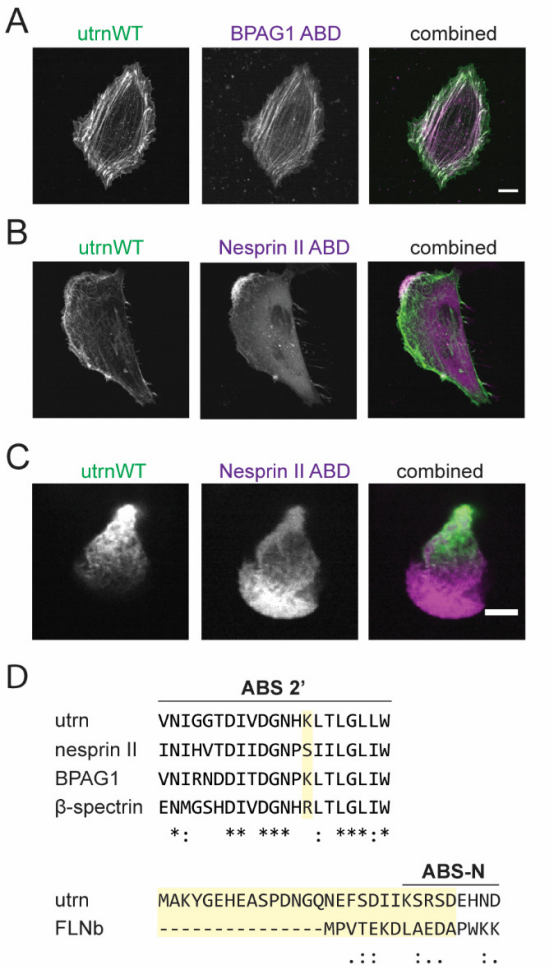

Figure 7: Native CH1-CH2 domains display different sub-cellular localizations.

(A) Localization of BPAG1 ABD (magenta) relative to utrnWT (green) in HeLa cells. (B) Localization of Nesprin II ABD (magenta) relative to utrnWT (green). (C) Localization of Nesprin II ABD (magenta) relative to utrnWT (green) in PLB cells. (D) Sequence alignment of native CH1-CH2 domains. Residue K121 for utrnWT highlighted in yellow (top) and the n-terminal region prior to CH1-CH2 and its truncation in yellow (bottom). Identical residues are annotated with '*', strongly conserved with ':', and weakly conserved with '.'.

SUPPLEMENTARY FIGURES

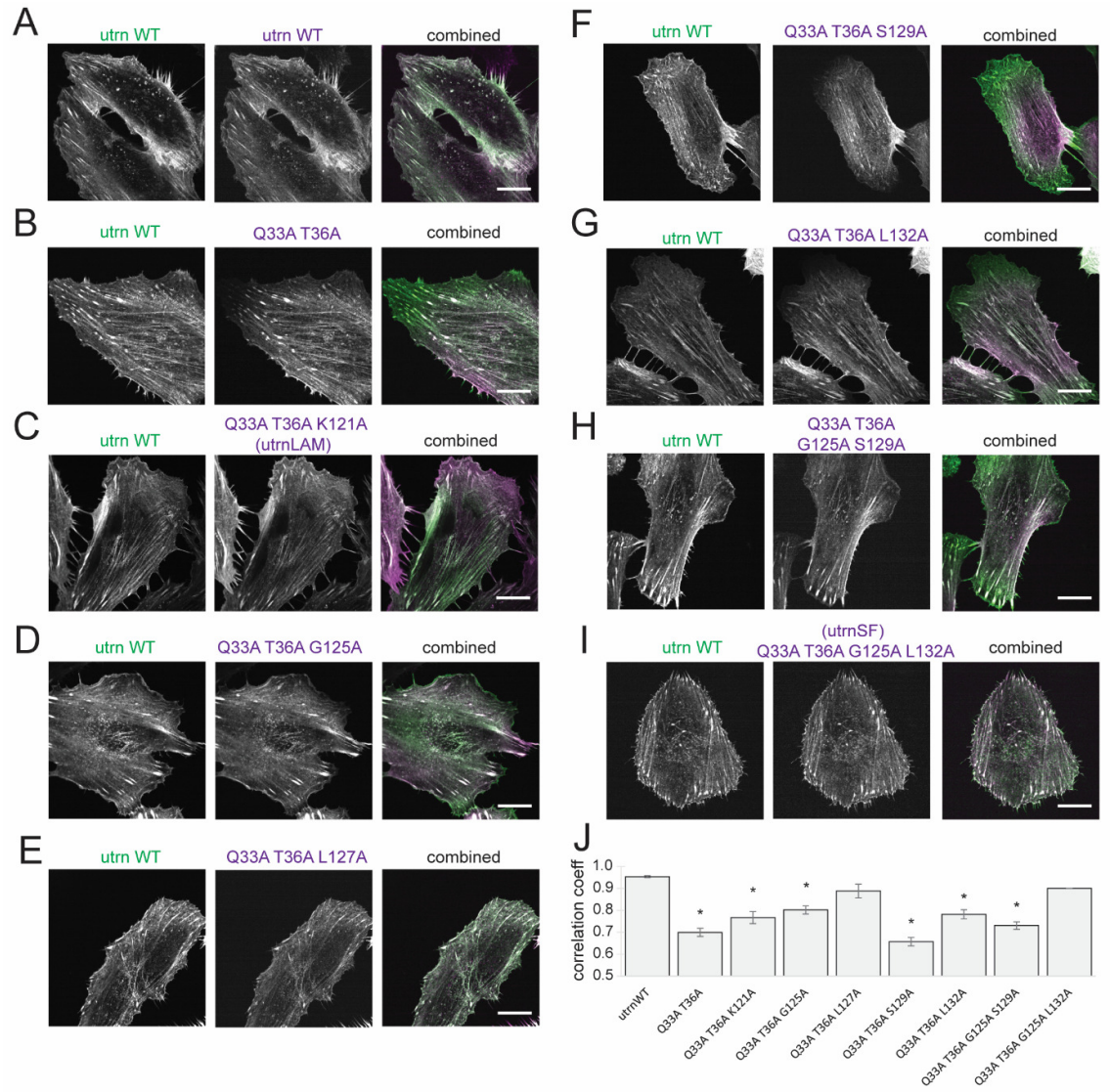

Figure S1: Localization screen of utrn CH1 mutants

(A-I) Localization of alanine mutations to different residues on utrn CH1 shown in HeLa cells. utrnWT is shown in green and the mutant in magenta. (J) Quantification of localization by Pearson's correlation coefficient for the two color channels.

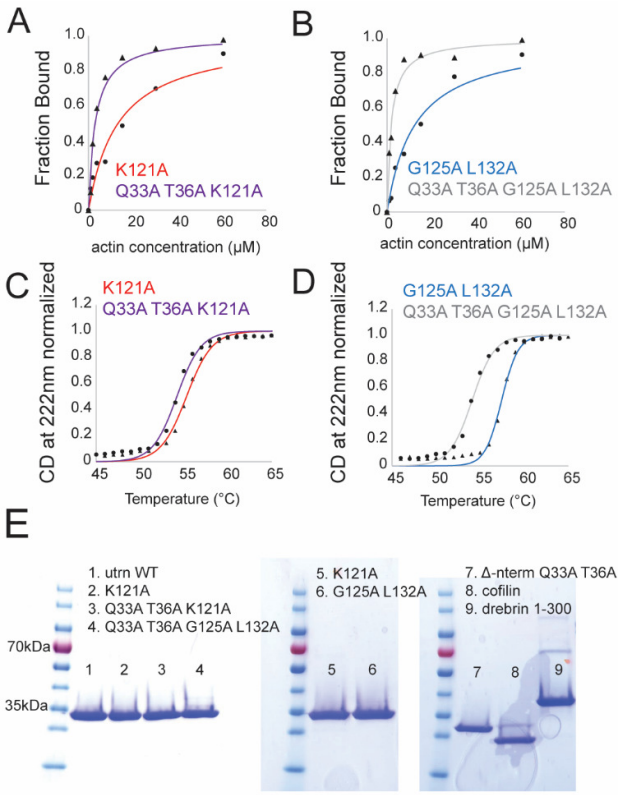

Figure S2: In vitro characterization of utrn CH1-CH2 mutants

(A) Cosedimentation measurements for K121A (red) and Q33A T36A K121A (purple). (B) Cosedimentation measurements for G125A L132A (blue) and Q33A T36A G125A L132A (grey). (C) Melting temperature curves for K121A (red) and Q33A T36A K121A (purple). (D) Melting temperature curves for G125A L132A (blue) and Q33A T36A G125A L132A (grey). (E) SDS page gels for the purified proteins.

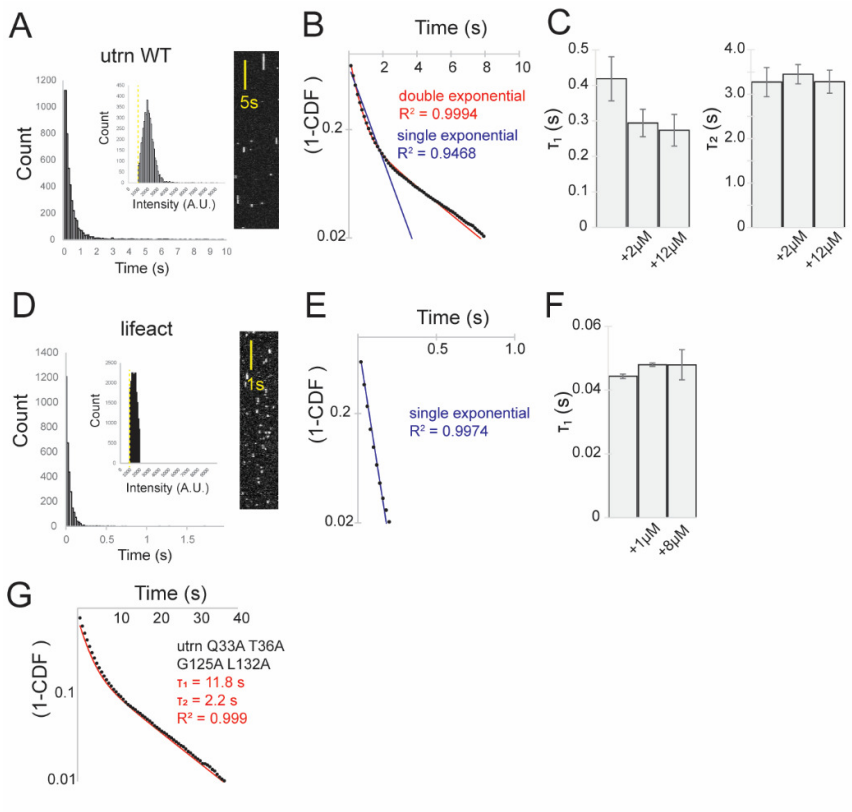

Figure S3: Calibration of single molecule binding kinetics

(A) Dwell time histogram, intensity histogram and kymograph for utrnWT. (B) Cumulative distribution function for utrnWT fit with either a single (blue) or double exponential decay (red). (C) Binding timescales as a function of protein concentration added. (D) Dwell time histogram, intensity histogram and kymograph for lifeact. (E) Cumulative distribution function for lifeact, fit with a single exponential. (F) Binding timescale as a function of concentration of protein added. (G) Cumulative distribution function for utrn Q33A T36A G125A L132A fit with a double exponential.

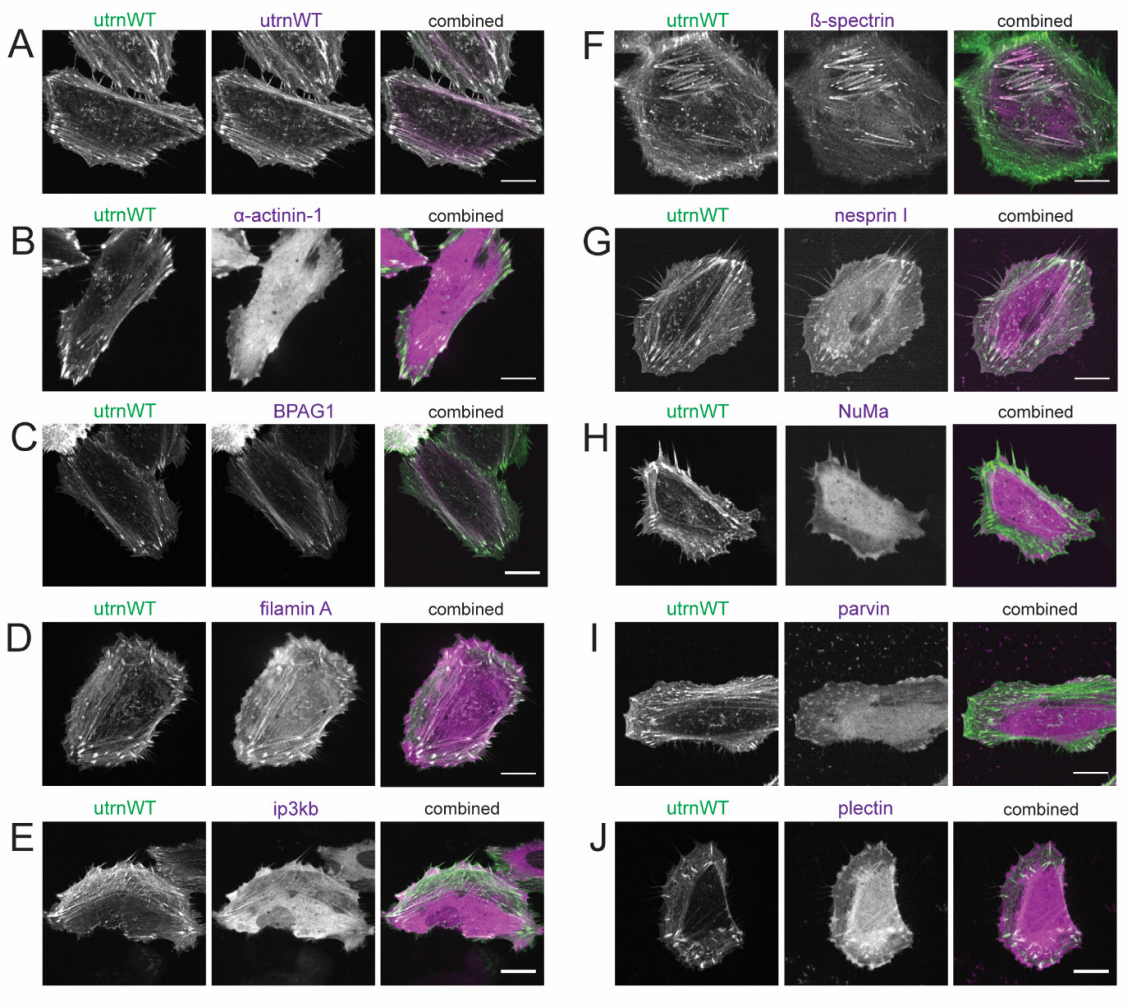

Figure S4: Localization of native CH1-CH2 domains

Localization of native CH1-CH2 domains shown in magenta relative to utrnWT shown in green. (A) utrnWT, (B) α-actinin 1, (C) BPAG1, (D) Filamin A, (E) ip3kb, (F) β-spectrin, (G) nesprin I, (H) NuMa, (I) parvin, (J) plectin.

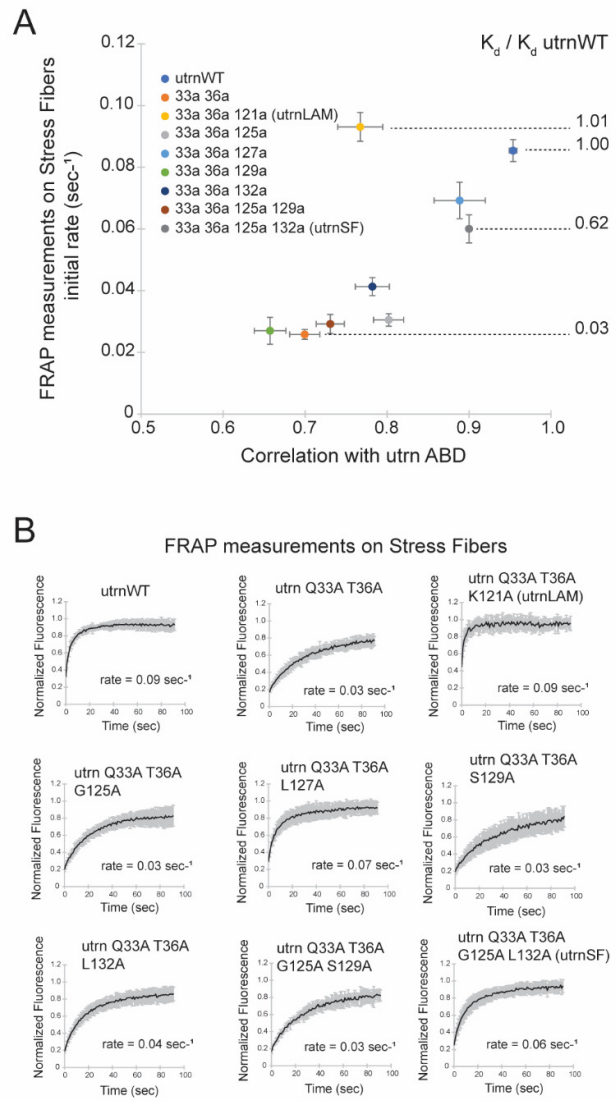

Figure S5: Comparison of localization and recovery rate on stress fibers for utrn CH1-CH2 mutants

(A) Comparison of Pearson's correlation coefficient and the initial recovery rate of different utrn CH1-CH2 mutants measured via Fluorescence Recovery After Photobleaching (FRAP) on stress fibers in HeLa cells. The relative binding affinity normalized to utrnWT is shown on the right. (B) FRAP recovery curves.

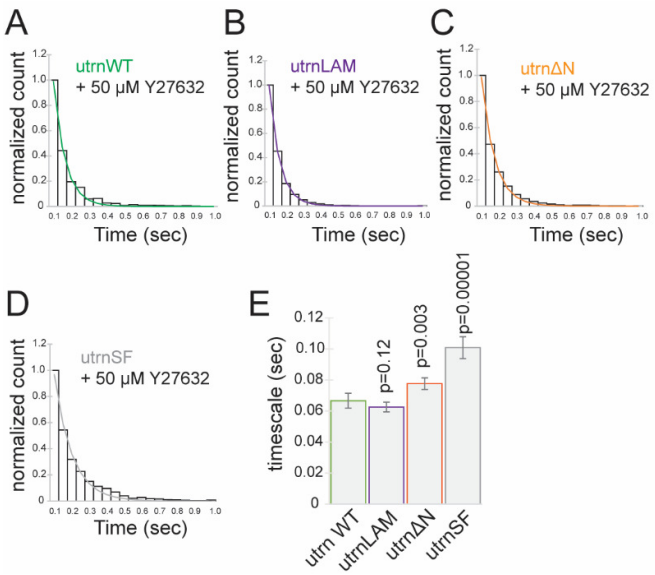

Figure S6: Kinetic measurements of utrn CH1-CH2 mutants in live cells

Single molecule dwell time histogram measured by photoactivation of utrophin mutant fusions to EOS in HeLa cells treated with 50μM Y27632 for (A) utrnWT, (B) utrnLAM, (C) utrnΔN and (D) utrnSF. (E) measurements of binding timescales for the different constructs.